Plasmonics
DOI 10.1007/s11468-015-0135-8

A Surface Design for Enhancement of Light Trapping Efficiencies in Thin Film Silicon Solar Cells

Cheng Sun[1] · Zhixiao Wang[1] · Xiaoqiu Wang[1] · Jie Liu[1]

Received: 12 August 2015 / Accepted: 28 October 2015

Abstract We report on a surface design of thin film silicon solar cells based on silver nanoparticle arrays and blazed grating arrays. The light transmittance is increased at the front surface of the cells, utilizing the surface plasmon resonance effect induced by silver nanoparticle arrays. As a reflection layer structure, blazed gratings are placed at the rear surface to increase the light reflectance at bottom of the thin film cells. With the combination of the silver nanoparticle arrays and the blazed gratings, the light trapping efficiency of the thin film solar cell is characterized by its light absorptance, which is determined from the transmittance at front surface and the reflectance at bottom, via the finite-difference time-domain (FDTD) numerical simulation method. The results reveal that the light trapping efficiency is enhanced as the structural parameters are optimized. This work also shows that the surface plasmon resonance effect induced by the silver nanoparticles and the grating characteristics of the blazed gratings play crucial roles in the design of the thin film silicon solar cells.

Keywords Surface plasmon · Thin film silicon solar cell · Silver nanoparticle array · Blazed grating · FDTD

✉ Xiaoqiu Wang
wangxqdl@sina.com

✉ Jie Liu
liujie_dlu@163.com

[1] College of Physical Science and Technology, Dalian University, 116622, Dalian, China

Introduction

In recent years, thin film silicon solar cells draw much attention because of their advantages in material costs and carrier collections [1–3]. However, the development of the thin film cells has been limited by the light absorption efficiency due to the finite thickness and the small absorption coefficients for photons at long wavelengths (e.g., ∼600–1100 nm). Therefore, advanced light trapping schemes have been proposed to improve the light absorption in the thin film cells. Generally, such light trapping schemes contain two categories: to reduce the light reflection at the front surface and to increase the optical path length (OPL) of light within the cells. Thus far, various light trapping technologies have been explored, including surface texturing [4, 5], antireflection coatings [6, 7], diffraction gratings[8, 9], photonic crystals [10, 11], and the top or bottom metallic nanoparticles based on surface plasmon [12, 13]. Among these technologies, many researches have been focused on plasmonic nanostructures. For instance, noble metal based nanostructures were investigated at the front surface of the cells, utilizing the scattering effect induced by the surface plasmon excitation of the metal particles, which performed a pronounced light concentration and absorption enhancement [14–21]. Besides, designs focused on the increase of the light's OPL were also reported. Among the various designs, the periodic grating structure is an important and simple method to effectively raise the OPL, because it can be placed on both surfaces of the thin film cells to enhance the light absorption in a broad wavelength range. For example, subwavelength grating structures have been used for ultra-broad band and omnidirectional antireflections [22–24]; studies of single front grating [25] and back rectangle metallic grating structures have also been reported [26, 27]. Recently, sev-

Published online: 14 November 2015

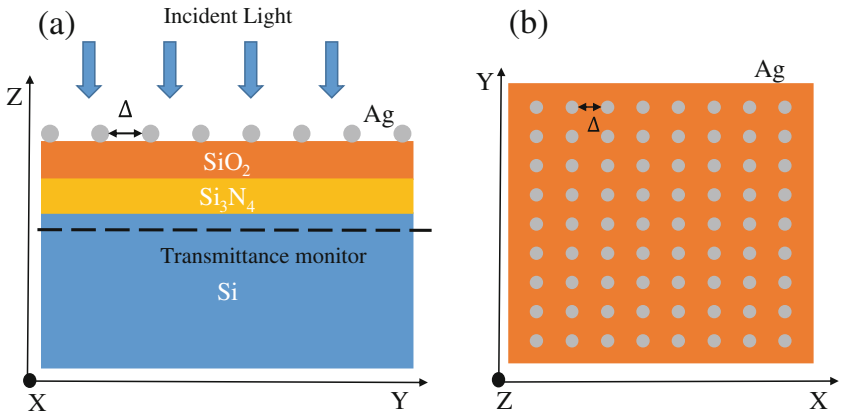

Fig. 1 Schematic of the structural design for the front surface of the thin film silicon solar cell, with a silver nanoparticle array being on top of a quarter wavelength layer of SiO_2/Si_3N_4: **a** cross section and **b** top view. In simulations, the light was normally incident from air. A plane monitor that measured the light transmittance into Si was placed in the $x - y$ plane and 100 nm away from the upper surface of Si, indicated in a *dashed line* in (**a**). The silver nanoparticles were evenly distributed in both dimensions in the $x - y$ plane, and the particle separation is labeled as Δ

eral studies have shown that blazed grating structures prove to be perfect reflectors as they can substantially enhance the OPL after tilting the angles of the diffraction beams away from the normal [28–31].

In this paper, we demonstrate a surface design of thin film silicon solar cells with a combination of silver nanoparticle arrays and blazed grating arrays. At the front surface of the cells, an antireflection layer structure is achieved by placing the silver nanoparticle arrays on top of quarter wavelength layers, utilizing the surface plasmon resonance effect of the metallic nanoparticles. At the rear surface, blazed grating arrays are used to enhance the light absorption by increasing the OPL of light within the cells. In this work, the light transmittance and reflectance at both surfaces have been studied in a wavelength range of 400–1000 nm via the finite-difference time-domain (FDTD) numerical simulation method, with a variety of structural parameters.

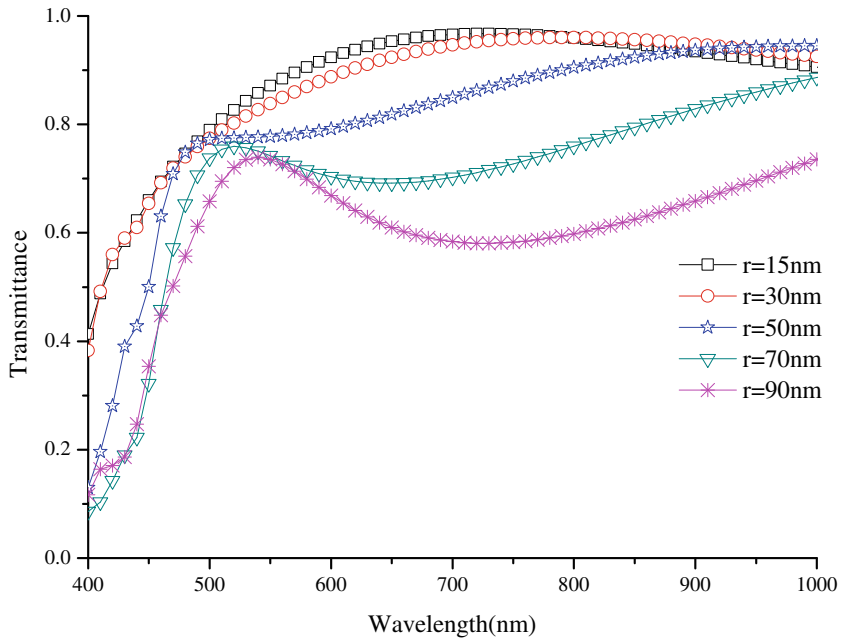

Fig. 2 Wavelength-dependent transmittance of light into Si for the design shown in Fig. 1. The radius of the silver nanoparticle was varied from $r = 15$ to 90 nm, with a fixed particle separation of $\Delta = 100$ nm

Numerical Simulation Method

In this work, the FDTD method was used to perform the calculations [32]. In all simulations, a plane-wave light with a wavelength range of 400–1000 nm was normally incident (shown as the z-axis indicated in Fig. 1). Periodic boundary conditions were employed in the $x - y$ plane in which silver nanoparticle arrays or blazed grating arrays were placed. In the z direction, perfect match layer boundary conditions were used. The mesh size was always kept smaller than 1/10 of the shortest wavelength studied in the region of non plasmon-carrying media to avoid the artifacts induced by the simulation method. The optical constants for all the media studied were from Palik's experimental data, as given in ref. [33] .

Front Surface: Silver Nanoparticle Arrays

In the design for the front surface of the thin film silicon solar cells, we combined silver nanopaticle arrays with an optimized quarter wavelength layer, and the detailed structure is shown in Fig. 1. As indicated in Fig. 1a, a silver nanoparticle array was placed on top of a quarter wavelength layer of SiO_2/Si_3N_4, at the front surface of silicon. The pre-optimized SiO_2/Si_3N_4 layer was employed as an antireflection layer, which has already been demonstrated to be effective in reducing the light reflectance at front surface of the cells, as shown in previous works [20, 21]. In the $x - y$ plane, the arrangement of the neighboring nanoparticles is shown in Fig. 1b, with the particle separation being labeled Δ.

To study the effects of the silver nanoparticle array on the light transmittance at the front surface, two structural parameters were varied: the particle separation, Δ, and the radius of the spherical silver particle, r. First, the particle radius was changed from r = 15 to 90 nm, while the particle separation was fixed at Δ = 100 nm, and the light transmittance as a function of the incident light's wavelength was simulated and the results are shown in Fig. 2. It is clear from Fig. 2 that the arrays with smaller individual nanoparticles (i.e., r = 15 and 30 nm) cause a greater light transmittance at most wavelengths studied. This is due to the surface plasmon resonance effect induced by the metallic nanoparticles; similar results were shown in the literatures [20, 21]. Note that different from the case of individual silver nanoparticles wherein the light transmittance enhancement can only occur at some particular wavelengths, the light transmittance in this design is enhanced in a broad-band fashion; this is due to the fact that the transmittance is not only effected by the surface plasmon resonance induced by the metallic nanoparticles but also by the grating properties associated with the silver nanoparticle arrays. Second, the particle separation was varied from Δ = 40 to 160 nm, while the particle radius was fixed at r = 50 nm, and the resulting transmittance curves are given in Fig. 3. It is evident from Fig. 3 that the arrays with larger particle separations (i.e., Δ = 140 and 160 nm) give rise to a greater transmitting performance. This is mainly because of the grating property of the array, that is, a larger separation allows a broader range of wavelength to pass through. The similar phenomenon was also reported in previous works [20, 21]. Figures 2 and 3 show that at the front surface of the cells, the light transmittance

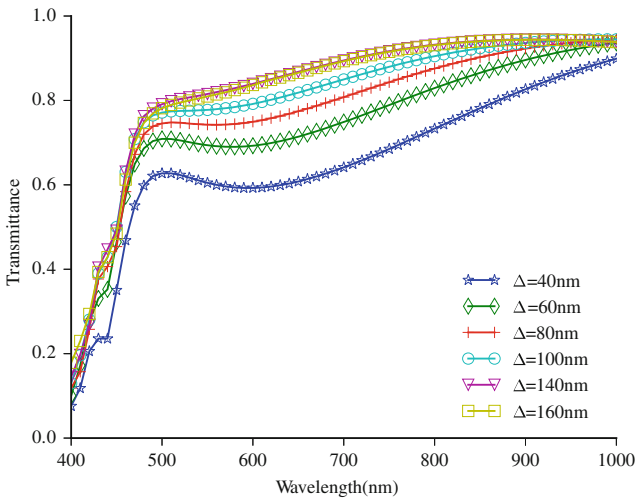

Fig. 3 Wavelength-dependent transmittance of light into Si for the design shown in Fig. 1. The particle separation was varied from Δ = 40 to 160 nm, with a fixed silver nanoparticle radius of r = 50 nm

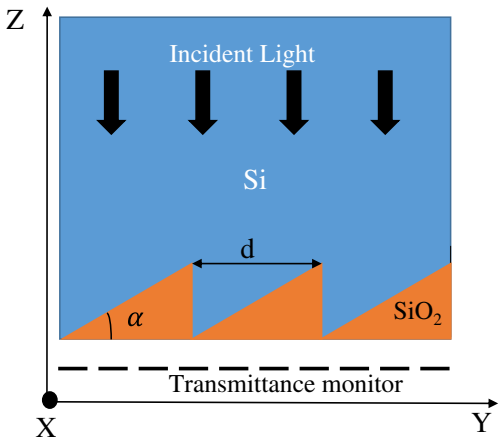

Fig. 4 Cross section of the structural design for the rear surface of the thin film silicon solar cells, with a blazed grating array being at the bottom of the Si layer. In simulations, the light was normally incident from Si. A plane monitor that measured the light transmittance away from Si was placed in the $x - y$ plane and 100 nm away from the bottom surface of Si. The blazed grating is infinite in the x axis, and the grating constant in the y axis is labeled d. The blaze angle is labeled α

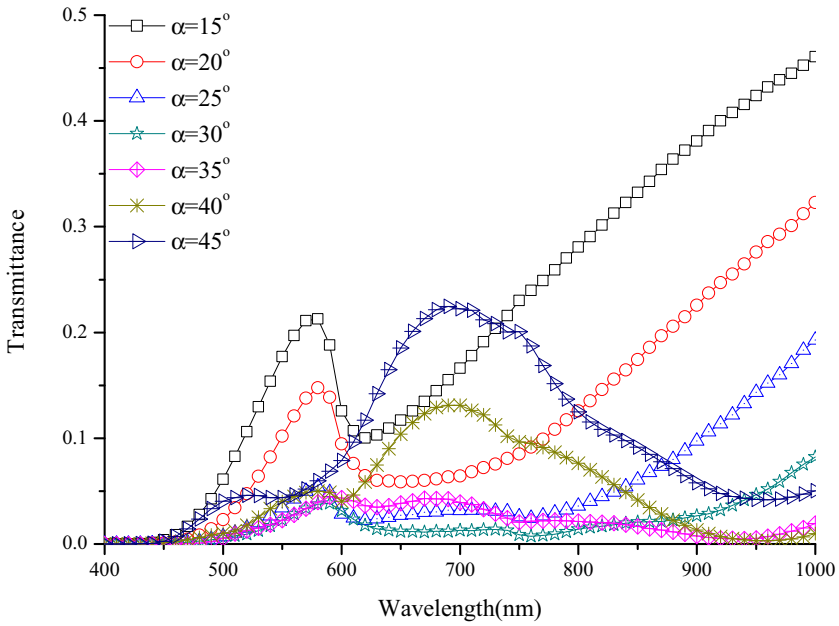

Fig. 5 Wavelength-dependent transmittance of light away from Si for the design shown in Fig. 4. The blaze angle was varied from α = 15 to 45°, with a fixed grating constant of d = 600 nm

may be increased by using silver nanoparticle arrays with small r or large Δ.

Rear Surface: Blazed Grating Arrays

Compared with their bulk counterparts, the thin film cells have a major shortcoming, that is, the incident light can easily penetrate through the silicon thin film without being utilized. To tackle this problem, a blazed grating array was placed at the bottom of the silicon layer to reduce the light transmittance at the rear surface of the thin film cells, and the schematic of the structural design for the rear surface is shown in Fig. 4. In this work, the material that constituted the blazed grating arrays was SiO_2. As indicated in Fig. 4, two structural parameters for the blazed grating were probed in this work: the blaze angle (labeled α, varying from 15 to 45°) and the grating constant (labeled d, varying from 400 to 1000 nm). In the simulations, the light source was placed inside the silicon layer and a plane monitor that measured the light transmittance (in the $x - y$ plane) was positioned

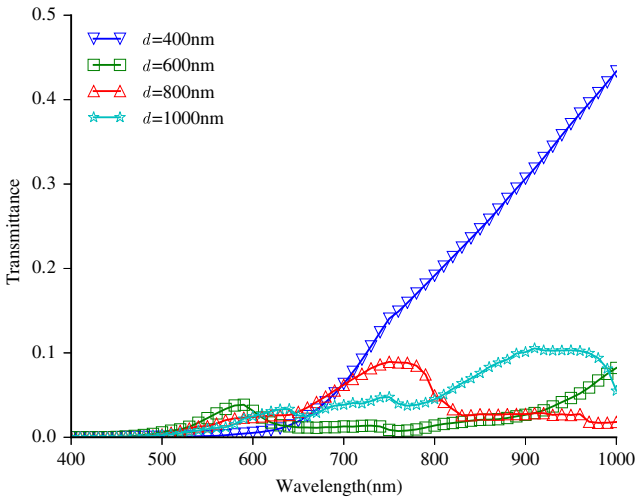

Fig. 6 Wavelength-dependent transmittance of light away from Si for the design shown in Fig. 4. The grating constant was varied from d = 400 to 1000 nm, with a fixed blaze angle of α = 30°

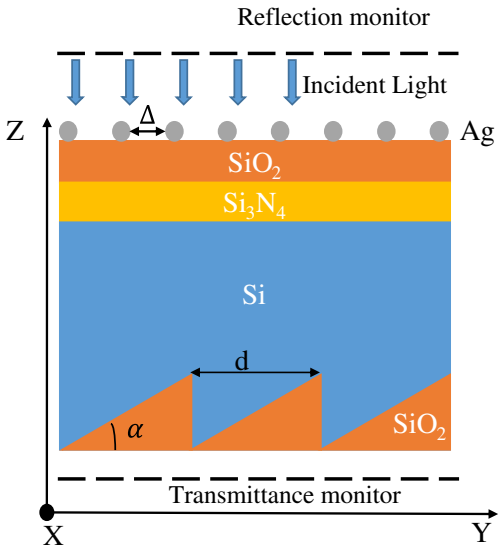

Fig. 7 Schematic of the structural design for the thin film silicon solar cell, with a silver nanoparticle array being at front and a blazed grating array at rear. In simulations, the light was normally incident from air. The silver nanoparticles were evenly distributed in both dimensions in the $x - y$ plane, and the particle separation is labeled Δ. The blazed grating is infinite in the x axis, and the grating constant in the y axis is labeled d

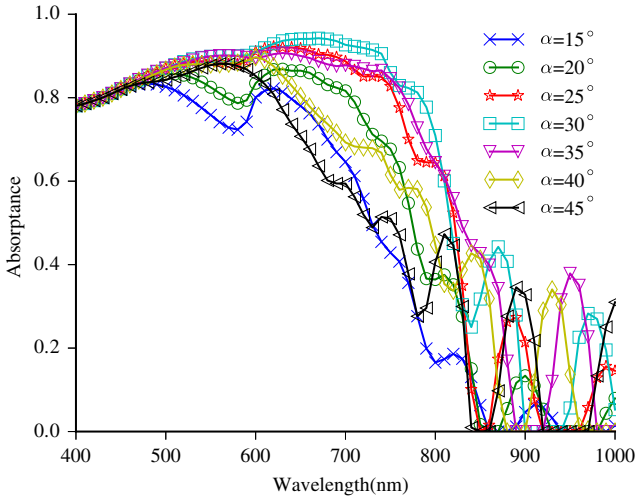

Fig. 8 Wavelength-dependent light absorptance by Si for the design shown in Fig. 7, determined from Eq. 1. At the front surface, the silver particle radius was r = 15 nm and the particle separation was Δ = 100 nm. At the rear surface, the grating constant was d = 600 nm, and the blaze angle was varied from α = 15 to 45°

outside the silicon layer and 100 nm away from the rear surface, as shown in Fig. 4.

For the rear surface, we first studied the effect of the blaze angle on the light transmittance, with a fixed grating constant of d = 600 nm; the results are shown in Fig. 5. It is observed from Fig. 5 that the blazed grating arrays with blaze angles of α = 30 and 35° result in lower transmittance curves at most wavelength studied. Note that different from the front surface, small values of transmittance are pursued at the rear surface. The observation in Fig. 5 demonstrates that the blaze angle cannot be either too small or too large, and that only certain angles can cause optimal transmitting performance. Furthermore, we also simulated the transmittance curves with a variety of grating constants in the condition of a fixed blaze angle (i.e., α = 35°), and the results are given in Fig. 6. It is clear from Fig. 6 that the lowest transmittance curve appears when the grating constant is d = 600 nm. From Figs. 5 and 6, we have learnt that the structural parameters of the blazed grating arrays at the rear surface need be optimized, and that in our case, it is α = 30 and 35° or d = 600 nm that shows a low transmittance curve.

Light Trapping Efficiency

After having separately studied the front and the rear surface of the cells, we combined the structural designs at both surfaces and characterized the light absorptance of the thin film cells, and the combined scheme is illustrated in Fig. 7. In the simulations, the thickness of the thin silicon layer was assumed 1 μm. As shown in Fig. 7, a plane monitor that measured the light reflectance was placed 100 nm away from the top of the cell, and another plane monitor that measured the light transmittance was put 100 nm away from the bottom of the cell. The reflectance of the incident light at the wavelength of λ from the front surface of the cell (labeled $R(\lambda)$) and the light transmittance at the rear surface (labeled $T(\lambda)$) were first determined. The light absorptance by Si (labeled $A(\lambda)$) was then calculated using Eq. 1, for a variety of structural parameters.

$$A(\lambda) = 1 - R(\lambda) - T(\lambda) \tag{1}$$

An exemplary figure of $A(\lambda)$ is given in Fig. 8 where the blaze angle was varied from α = 15 to 45°, while the other structural parameters were fixed to be Δ = 100 nm, r = 15 nm, and d = 600 nm. By examining Fig. 8, it is observed that the blaze angles of α = 30° and α = 35° are slightly better than the others at shorter wavelengths (e.g., <800 nm). While the absorptance curves become oscillatory at longer wavelengths (e.g., >800 nm) and it is difficult to tell which one is better. Note that when changing the other structural parameters (i.e., Δ, r, or d), the corresponding absorptance curves (not shown in this paper) also present similar oscillatory behaviours. Therefore, other than the light absorptance at each wavelength, it is more appropriate to use the weighted mean values of the photons absorbed by Si over all the wavelengths, to quantify the light trapping

Table 1 Weighted mean values of the photons absorbed by Si, $\xi_{AM1.5}$, with a fixed particle separation of Δ = 100 nm for the silver nanoparticle array and a fixed grating constant of d = 600 nm for the blazed grating array

	r = 15 nm	r = 30 nm	r = 50 nm	r = 70 nm	r = 90 nm
α = 15°	0.5668	0.5653	0.5323	0.4653	0.4477
α = 20°	0.6407	0.6370	0.5884	0.5023	0.4746
α = 25°	0.7096	0.7060	0.6431	0.5374	0.4998
α = 30°	0.7467	0.7462	0.6753	0.5546	0.5103
α = 35°	0.7284	0.7287	0.6627	0.5453	0.5040
α = 40°	0.6627	0.6633	0.6148	0.5179	0.4858
α = 45°	0.6110	0.6125	0.5782	0.4979	0.4710

The radius of the silver nanoparticle was varied from r = 15 to 90 nm, and the blaze angle was varied from α = 15 to 45°

Table 2 Weighted mean values of the photons absorbed by Si, $\xi_{AM1.5}$, with a fixed particle radius of r = 50 nm for the silver nanoparticle array and a fixed grating constant of d = 600 nm for the blazed grating array

	Δ = 40 nm	Δ = 60 nm	Δ = 80 nm	Δ = 100 nm	Δ = 140 nm	Δ = 160 nm
$\alpha = 15°$	0.4022	0.4701	0.5059	0.5323	0.5572	0.5514
$\alpha = 20°$	0.4336	0.5126	0.5559	0.5884	0.6203	0.6141
$\alpha = 25°$	0.4641	0.5541	0.6048	0.6431	0.6815	0.6749
$\alpha = 30°$	0.4803	0.5774	0.6332	0.6753	0.7175	0.7106
$\alpha = 35°$	0.4722	0.5674	0.6219	0.6627	0.7030	0.6961
$\alpha = 40°$	0.4484	0.5333	0.5803	0.6148	0.6476	0.6412
$\alpha = 45°$	0.4327	0.5092	0.5494	0.5782	0.6045	0.5984

The particle separation was varied from Δ = 40 to 160 nm, and the blaze angle was varied from α = 15 to 45°

efficiency of the cells. The weighted mean, $\xi_{AM1.5}$, is given by

$$\xi_{AM1.5} = \frac{\int_{\lambda_1}^{\lambda_2} A(\lambda)N(\lambda)d\lambda}{\int_{\lambda_1}^{\lambda_2} N(\lambda)d\lambda} \tag{2}$$

where λ is the wavelength of the incident light, and λ_1 and λ_2 are the wavelengths of the lower and upper boundaries, respectively. In this work, λ_1 = 400 nm and λ_2 = 1000 nm. $N(\lambda)$ is the solar spectrum, which is the distribution of photon numbers as a function of wavelength, under the standard testing condition (AM1.5, 100 mW/cm^2 and 25 °C). $N(\lambda)$ is given by

$$N(\lambda) = \frac{W(\lambda)}{E(\lambda)} = \frac{W(\lambda)\lambda}{hc} \tag{3}$$

where $W(\lambda)$ is the corresponding solar spectral irradiance at the wavelength of λ, $E(\lambda)$ is the photon energy at λ, h = 6.6261 × 10^{-34}Js and c =3×10^8m/s. $N(\lambda)$ was calculated from Eq. 3 by using the ASTM G173-03 reference solar spectral irradiance (global tilt), $W(\lambda)$.

As mentioned above, the light absorptance by Si, $A(\lambda)$, was determined from Eq. 1 by the light reflectance at front, $R(\lambda)$, and the transmittance at rear, $T(\lambda)$, for a variety of structural parameters. With the values of $N(\lambda)$ and $A(\lambda)$, we computed $\xi_{AM1.5}$ from Eq. 2 under various combinations of the structural parameters for the silver nanoparticle arrays at the front surface (i.e., Δ and r) and the blazed grating arrays at the rear surface (i.e., α and d). The corresponding results are respectively shown in Table 1 through Table 4.

Table 1 represents the weighted mean values of the photons absorbed by silicon when the silver particle separation and the grating constant of the blazed grating were fixed (i.e., Δ = 100 nm and d = 600 nm), while the radius of the silver nanoparticle, r, and the blaze angle of the blazed grating, α were varied. It is apparent from Table 1 that the structure with the combination of a small silver particle size (i.e., r = 15 or 30 nm) at top and a blaze angle of α = 30 or 35° at bottom gives rise to a great light trapping efficiency (i.e., $\xi_{AM1.5} > 0.72$) for the solar cell. The maximum value of $\xi_{AM1.5}$ appears to be 0.7467 when r = 15 nm and α = 30°. This result is the combination of the high transmittance at the front surface with a small size of the silver nanoparticle (indicated in Fig. 2) and the low transmittance at the rear surface with the blaze angle of α = 30 or 35° (indicated in Fig. 5).

Similarly, Table 2 shows the values of $\xi_{AM1.5}$ by respectively changing the silver particle separation, Δ, at front and the blaze angle, α, at bottom, while maintaining the other parameters (i.e., r = 50 nm and d = 600 nm). It is evident from Table 2 that the optimal value of $\xi_{AM1.5}$ occurs when the particle separation is as large as Δ = 140 nm or 160 nm as well as the blaze angle is α = 30 or 35°. This is consistent with the previous findings that the large particle separation causes a greater light transmittance at the front surface, which was revealed by Fig. 3.

To further optimize the surface design of the cells, the $\xi_{AM1.5}$ values under two other combinations of the four

Table 3 Weighted mean values of the photons absorbed by Si, $\xi_{AM1.5}$, with a fixed particle separation of Δ = 100 nm for the silver nanoparticle array and a fixed blaze angle of $\alpha = 30°$ for the blazed grating array

	r = 15 nm	r = 30 nm	r = 50 nm	r = 70 nm	r = 90 nm
d = 400 nm	0.6583	0.6533	0.6065	0.5236	0.4968
d = 600 nm	0.7467	0.7462	0.6753	0.5546	0.5103
d = 800 nm	0.7039	0.7033	0.6447	0.5379	0.5008
d = 1000 nm	0.7024	0.6983	0.6371	0.5348	0.4997

The radius of the silver nanoparticle was varied from r = 15 to 90 nm, and the grating constant was varied from d = 400 to 1000 nm

Table 4 Weighted mean values of the photons absorbed by Si, $\xi_{AM1.5}$, with a fixed particle radius of $R = 50$ nm for the silver nanoparticle array and a fixed blaze angle of $\alpha = 30°$ for the blazed grating array

	$\Delta = 40$ nm	$\Delta = 60$ nm	$\Delta = 80$ nm	$\Delta = 100$ nm	$\Delta = 140$ nm	$\Delta = 160$ nm
$d = 400$ nm	0.4507	0.5309	0.5742	0.6065	0.6380	0.6317
$d = 600$ nm	0.4801	0.5774	0.6332	0.6753	0.7175	0.7106
$d = 800$ nm	0.4649	0.5557	0.6067	0.6447	0.6819	0.6752
$d = 1000$ nm	0.4608	0.5495	0.5994	0.6371	0.6749	0.6682

The particle separation was varied from $\Delta = 40$ to 160 nm, and the grating constant was varied from $d = 400$ to 1000 nm

structural parameters were also calculated: (I) r and d were varied while Δ and α were fixed, and the corresponding $\xi_{AM1.5}$ values are tabulated in Table 3; (II) Δ and d were varied while r and α were fixed, and the results are given in Table 4. Referring to Table 3, the two largest $\xi_{AM1.5}$ values in case I are measured to be $\xi_{AM1.5} = 0.7467$ for $r = 15$ nm and $d = 600$ nm, and $\xi_{AM1.5} = 0.7462$ for $r = 30$ nm and $d = 600$ nm. It can be seen from Table 4 that the largest values of $\xi_{AM1.5}$ in case II appear to be $\xi_{AM1.5} = 0.7175$ for $\Delta = 140$ nm and $d = 600$ nm, and $\xi_{AM1.5} = 0.7106$ for $\Delta = 160$ nm and $d = 600$ nm. The results observed from Tables 3 and 4 reveal that the light trapping efficiency is optimized when the grating constant of the blazed grating array at bottom is as large as 600 nm, which is in good agreement with the previous observation indicated in Fig. 6.

Conclusions

Based on silver nanoparticle arrays and blazed grating arrays, we have designed structures of thin film silicon solar cells both at the front and the rear surfaces. In the design of the front surface of the cells, silver nanoparticle arrays have been placed in order to increase the light transmittance at top, utilizing the surface plasmon resonance effect induced by the metallic nanoparticles. At the rear surface of the cells, blazed grating arrays have been used to decrease light transmittance at bottom. We have also combined both surface designs and calculated the weighted mean values of the photons absorbed by silicon over all the wavelengths studied. The results indicate that the light trapping efficiency can be optimized under certain combinations of the structural parameters. For instance, the weighted mean value as great as $\xi_{AM1.5} = 0.7467$ can be achieved when the parameters are $\Delta = 100$ nm, $r = 15$ nm, $\alpha = 30°$, and $d = 600$ nm. The surface design proposed in this work may be implemented in practice to enhance the light trapping efficiencies of the thin film silicon solar cells.

Acknowledgments C. Sun acknowledges support by Grant Number 31400718 from the National Natural Science Foundation of China.

References

1. Macdonald D, Cuevas A, Kerr MJ, Samundsett C, Ruby D, Winderbaum S, Leo A (2004) Texturing industrial multicrystalline silicon solar cells. Sol Energy 76(1):277–283
2. Boltasseva A, Atwater HA (2011) Low-loss plasmonic metamaterials. Science 331:290–291
3. Atwater HA, Polman A (2010) Plasmonics for improved photovoltaic devices. Nat Mater 9(3):205–213
4. Qiu Y, Wang L, Hao H, Shi W, Lu M (2015) A synergetic effect of surface texture and field-effect passivations on improving si solar cell performance. Physica E: Low-dimensional Systems and Nanostructures 71:96–100
5. Lanz T, Lapagna K, Altazin S, Boccard M, Haug F-J, Ballif C, Ruhstaller B (2015) Light trapping in solar cells: numerical modeling with measured surface textures. Opt Eng 23(11):A539–A546
6. Li D, Kunz T, Wolf N, Liebig JP, Wittmann S, Ahmad T, Hessmann MT, Auer R, Göken M, Brabec CJ (2015) Silicon nitride and intrinsic amorphous silicon double antireflection coatings for thin-film solar cells on foreign substrates. Thin Solid Films 583:25–33
7. Rajbhandari PP, Emrani A, Dhakal TP, Westgate CR, Klotzkin D (2014) Antireflection coatings designed by the average uniform algorithm for thin film solar cells. Appl Opt 53(34):8006–8011
8. Dubey R, Saravanan S, Kalainathan S (2014) Performance enhancement of thin film silicon solar cells based on distributed bragg reflector & diffraction grating. AIP Adv 4(12):127121
9. Sidharthan R, Murukeshan V (2013) Improved light absorption in thin film solar cell using combination of gap modes and grating back reflector. Thin Solid Films 548:581–584
10. Mutitu JG, Shi S, Chen C, Creazzo T, Barnett A, Honsberg C, Prather DW (2008) Thin film solar cell design based on photonic crystal and diffractive grating structures. Opt Express 16(19):15238–15248
11. Zhang A, Guo Z, Tao Y, Wang W, Mao X, Fan G, Zhou K, Qu S (2015) Advanced light-trapping effect of thin-film solar cell with dual photonic crystals. Nanoscale Res Lett 10(1):1–10
12. Diukman I, Orenstein M (2011) How front side plasmonic nanostructures enhance solar cell efficiency. Sol Energy Mater Sol Cells 95(9):2628–2631
13. Winans JD, Hungerford C, Shome K, Rothberg LJ, Fauchet PM (2015) Plasmonic effects in ultrathin amorphous silicon solar cells: performance improvements with ag nanoparticles on the front, the back, and both. Opt Express 23(3):A92–A105
14. Moulin E, Sukmanowski J, Schulte M, Gordijn A, Royer F, Stiebig H (2008) Thin-film silicon solar cells with integrated silver nanoparticles. Thin Solid Films 516(20):6813–6817
15. Rockstuhl C, Lederer F (2009) Photon management by metallic nanodiscs in thin film solar cells. Appl Phys Lett 94 (21):213102
16. Akimov YA, Ostrikov K, Li E (2009) Surface plasmon enhancement of optical absorption in thin-film silicon solar cells. Plasmonics 4(2):107–113

17. Mokkapati S, Beck F, Polman A, Catchpole K (2009) Designing periodic arrays of metal nanoparticles for light-trapping applications in solar cells. Appl Phys Lett 95 (5):053115
18. Islam K, Alnuaimi A, Battal E, Okyay AK, Nayfeh A (2014) Effect of gold nanoparticles size on light scattering for thin film amorphous-silicon solar cells. Sol Energy 103:263–268
19. Lee Y-Y, Ho W-J, Chen Y-T (2014) Performance of plasmonic silicon solar cells using indium nanoparticles deposited on a patterned tio 2 matrix. Thin Solid Films 570:194–199
20. Sun C, Su J, Wang X (2015) A design of thin film silicon solar cells based on silver nanoparticle arrays. Plasmonics 10(3):633–641
21. Sun C, Wang X (2015) Efficient light trapping structures of thin film silicon solar cells based on silver nanoparticle arrays. Plasmonics:1–8
22. Kanamori Y, Sasaki M, Hane K (1999) Broadband antireflection gratings fabricated upon silicon substrates. Opt Lett 24(20):1422–1424
23. Striemer C, Fauchet P (2002) Dynamic etching of silicon for broadband antireflection applications. Appl Phys Lett 81(16):2980–2982
24. Song YM, Bae SY, Yu JS, Lee YT (2009) Closely packed and aspect-ratio-controlled antireflection subwavelength gratings on gas using a lenslike shape transfer. Opt Lett 34(11):1702–1704
25. Song YM, Yu JS, Lee YT (2010) Antireflective submicrometer gratings on thin-film silicon solar cells for light-absorption enhancement. Opt lett 35(3):276–278
26. Bai W, Gan Q, Bartoli F, Zhang J, Cai L, Huang Y, Song G (2009) Design of plasmonic back structures for efficiency enhancement of thin-film amorphous Si solar cells. Opt lett 34(23):3725–3727
27. Escoubas L, Simon J-J, Torchio P, Duché D, Vedraine S, Vervisch W, Le Rouzo J, Flory F, Rivière G, Yeabiyo G et al (2011) Bringing some photonic structures for solar cells to the fore. Appl Opt 50(9):C329–C339
28. Zheng G, Zhang W, Xu L, Chen Y, Liu Y (2014) Absorbance enhancement of thin film solar cells with front double dielectric and back metallic grating. Infrared Phys Technol 67:52–57
29. Zhang W, Zheng G, Jiang L, Li X (2013) Combined front diffraction and back blazed gratings to enhance broad band light harvesting in thin film solar cells. Opt Commun 298:250–253
30. Lin LJ, Chiou Y-P (2012) Improving thin-film crystalline silicon solar cell efficiency with back surface field layer and blaze diffractive grating. Solar Energy 86(5):1485–1490
31. Ji L, Varadan V (2012) A blazed grating for light trapping in a-si thin-film solar cells. J Opt 14(9):095001
32. Lumerical Solutions, Inc., http://www.lumerical.com/tcad-products/fdtd/
33. Palik ED (1998) Handbook of optical constants of solids, Vol 3. Academic press